Available online at www.sciencedirect.com

ScienceDirect

journal homepage: www.elsevier.com/locate/he

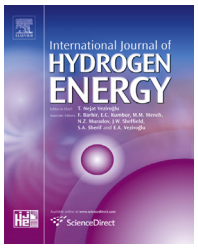

One-pot synthesis of graphene/carbon nanospheres/graphene sandwich supported Pt_3Ni nanoparticles with enhanced electrocatalytic activity in methanol oxidation

Wenhan Niu [a], *Ligui Li* [a,**], *Xiaojun Liu* [a], *Weijia Zhou* [a], *Wei Li* [a], *Jia Lu* [a], *Shaowei Chen* [a,b,*]

[a] *New Energy Research Institute, College of Environment and Energy, South China University of Technology, Guangzhou Higher Education Mega Center, Guangzhou 510006, China*

[b] *Department of Chemistry and Biochemistry, University of California, 1156 High Street, Santa Cruz, CA 95064, United States*

ARTICLE INFO

Article history:
Received 10 November 2014
Received in revised form
20 February 2015
Accepted 23 February 2015
Available online 16 March 2015

Keywords:
Pt3Ni alloy nanoparticle
Carbon nanosphere
Graphene
Sandwich structure
Methanol oxidation
Carbon monoxide

ABSTRACT

A facile method was demonstrated for the preparation of Pt_3Ni alloy nanoparticles supported on a sandwich-like graphene sheets/carbon nanospheres/graphene sheets substrate (Pt_3Ni–C/rGO) through a one-pot solvothermal process in N,N-dimethylformide without the addition of reducing agents and surfactants. Transmission electron microscopic measurements showed that carbon nanospheres were homogeneously dispersed in the matrix of exfoliated graphene sheets, and Pt_3Ni nanoparticles were distributed on the graphene surfaces without apparent agglomeration, where the average core size was estimated to be 12.6 ± 2.4 nm. X-ray photoelectron spectroscopic studies demonstrated that electron transfer likely occurred from the Pt_3Ni alloy nanoparticles to the graphene sheets. Electrochemical measurements showed that the mass activity of the Pt_3Ni–C/rGO catalysts in methanol oxidation was 1.7-times higher than that of Pt_3Ni nanoparticles supported on reduced graphene oxide alone (Pt_3Ni/rGO), and 1.3-times higher than that of commercial Pt/C (20 wt%). Additionally, CO tolerance and durability were also remarkably enhanced. These superior electrocatalytic activities were attributed to the following major factors: (i) the insertion of carbon nanospheres into the graphene matrix prevented restacking/refolding of the graphene sheets, leading to an increasing number of accessible active sites as well as transport channels for mass and charges; and (ii) the synergetic effect between Pt_3Ni nanoparticles and rGO weakened the bonding interactions with reactant species, as manifested by the enhanced kinetics of methanol oxidation and CO oxidative desorption.

* *Corresponding author*. Department of Chemistry and Biochemistry, University of California, 1156 High Street, Santa Cruz, California 95064, United States.

** *Corresponding author*.

E-mail addresses: esguili@scut.edu.cn (L. Li), shaowei@ucsc.edu (S. Chen).

http://dx.doi.org/10.1016/j.ijhydene.2015.02.095

Introduction

Direct methanol fuel cells (DMFCs) have been attracting considerable attention for their potential applications in vehicle power supplies and portable electronic devices. Platinum has been used extensively as anode materials in DMFCs due to its high electrocatalytic activity for direct methanol oxidation [1–4]. However, the limited reserves and high costs of platinum have been the main bottlenecks that hamper the widespread commercialization of DMFCs [5–9]. Preparation Pt-based alloy nanoparticles with non-precious metals (e.g., Fe, Ni, Co, Sn, etc.) is a judicious strategy which can not only reduce the amount of Pt used, but also lead to substantial enhancement of the electrocatalytic activity resulting from the synergetic effect between Pt and non-precious metals [10–16]. More importantly, alloy nanoparticles may display stronger resistance to CO poisoning thanks to deliberate tuning of the d-electron density of Pt [17,18]. Among the alloy electrocatalysts, Pt_3Ni is of great interest, as it has been reported by Stamenkovic et al. that the $Pt_3Ni(111)$ surface is 10 times more active for oxygen reduction reaction (ORR) than the corresponding Pt(111) surface [19] and 90 times more active than leading commercial Pt/C catalysts [20–24]. Theoretical simulation has also shown that phase separation that generally lead to Pt surface enrichment is unlikely to occur in the Pt–Ni alloy system [14,25,26]. In addition, with a nickel hydroxide passivated surface as well as enhanced stability of Ni in the Pt lattice, Ni in Pt–Ni alloys is much more difficult to dissolve in typical fuel cell electrolytes than Ru in the extensively used PtRu alloys in the potential range of methanol oxidation [14].

In practical applications, nanoparticle catalysts are usually dispersed on supporting substrates of high surface areas or protected by organic surfactants to prevent aggregation and hence enhance accessibility [27–29]. From the viewpoint of both academic research and practical applications, carbon-based materials have been one of the most commonly used supporting substrates, such as carbon black [30], carbon nanotubes [31], and graphene [32–34]. This is mainly due to their low costs, high conductivity, and remarkable chemical inertness that may facilitate electron-transfer reactions on the electrode surface and concurrently improve catalyst stability and durability. Of the carbon-based materials, graphene derivatives have attracted worldwide attention in fuel cell electrocatalysis [27]. Currently, graphene (oxide) is mostly prepared by the Hummers method, which is then subjected to chemical reduction with strong reducing agents, such as hydrazine and $NaBH_4$, to (partly) restore the Csp^2 hybridization. Unfortunately, the resulting reduced graphene oxide (rGO) sheets might refold/restack because of strong $\pi-\pi$ interactions, thus compromising the even dispersion and ready accessibility of supported metal nanoparticle catalysts.

Whereas restacking of graphene sheets may be diminished by using capping ligands/surfactant agents, the capping ligands/surfactant agents also block the active sites of nanoparticle catalysts and hence decrease the catalytic activity [35–37]. Therefore, it remains highly desired to develop new graphene-based supporting substrates with unique micro/nano structures for nanoparticle catalysts so that their electrocatalytic performance can be fully achieved.

Herein, we describe a facile method to synthesize surfactant-free Pt_3Ni nanoparticles supported on sandwich-like graphene/carbon sphere/graphene substrates (Pt_3Ni–C/rGO) for the electrocatalytic oxidation of methanol. It was found that the obtained Pt_3Ni–C/rGO composites showed much greater peak current density, remarkably higher mass and specific activity, as well as better CO tolerance and durability in methanol oxidation than the same alloy nanoparticles supported on rGO alone (Pt_3Ni/rGO) and commercial Pt/C catalysts. The superior catalytic activity indicate that the insertion of carbon nanospheres into graphene sheets may be a general and effective method to minimize the aggregation of graphene nanosheets and enhance the electrocatalytic activity of nanoparticle catalysts in the anodic oxidation of methanol.

Experimental section

Chemicals

Platinum(II) 2,4-pentanedionate ($[Pt(acac)_2]$, 97%), nickel(II) 2,4-pentanedionate ($[Ni(acac)_2]$, 95%), graphite powders (99.998%, 8000 mesh), and Nafion (5% w/w) were purchased from Aladdin Reagents Inc. Vulcan XC-72 active carbon nanospheres were purchased from Cabot Corporation. All other reagents were of analytical grade and used without further purification.

Synthesis of nanocomposite catalysts

Pt_3Ni/rGO was prepared by the following procedure. In a typical reaction, graphene oxide (GO) was first synthesized by a modified Hummers method [38], and dispersed in N,N-dimethylformide (DMF) to form a GO solution at a concentration of 0.5 mg/mL. 1 mL of a solution containing 30 mM $Pt(acac)_2$ and 10 mM $Ni(acac)_2$ was then mixed (Pt:Ni molar feed ratio 3:1) with 16 mL of the GO solution in DMF in a sealed PTFE-lined vessel under sonication for 30 min. The resulting mixture was transferred into a furnace and heated at 180 °C for 6 h before being cooled down to room temperature. Finally, the product was sonicated for 30 min and then washed several times with an ethanol-acetone mixture to remove excessive reagents. The obtained catalysts were dried in a vacuum oven at 60 °C overnight, and denoted as Pt_3Ni/rGO.

Pt_3Ni–C/rGO was synthesized in a similar fashion except that graphene/carbon/graphene (GCG) sandwiched-like composite substrates were used instead, which were prepared by mixing GO and active carbon at a 3:1 mass ratio in deionized water under sonication for 30 min, before being precipitated by centrifugation and dried in a vacuum oven at 60 °C overnight.

Characterizations

Transmission electron microscopic (TEM) measurements were conducted on a Tecnai G2-F20 at an acceleration voltage

of 100 kV, along with EDX analysis. The TEM samples were prepared by drop-casting a water solution containing the nanocomposite catalysts directly onto a copper grid coated with a holy carbon film. X-ray photoelectron spectroscopic (XPS) measurements were performed on a Thermo Escalab 250Xi instrument. The binding energies were calibrated by using C1s (284.6 eV) as the reference energy. Powder X-ray diffraction (XRD) patterns were recorded with a Bruker D8-Advance diffractometer using Cu Kα radiation. Raman spectra were recorded on an RENISHAW inVia instrument with an Ar laser source of 488 nm in a macroscopic configuration.

Electrochemistry

Electrochemical measurements were performed on a CHI 750E electrochemical workstation (CH Instruments, Chenhua Co., China) in a conventional three-electrode cell, with a platinum wire as the counter electrode, a reversible hydrogen electrode (RHE) as the reference electrode, and a catalysts-modified glassy carbon electrode as the working electrode. To prepare the catalysts-modified electrode, 1 mg of the catalysts was added into a solution containing water, isopropanol and Nafion (5%) at a volume ratio of 4:1:0.025 to form a homogeneous suspension at a catalyst concentration of 1 mg/mL. A calculated amount (20 μL for the Pt/C 20 wt% catalyst; 10 μL for the Pt_3Ni/rGO and Pt_3Ni–C/rGO catalysts) of the suspension was then evenly cast on the clean glassy carbon electrode (GCE) with a syringe and dried in air, corresponding to a Pt loading of each catalyst at 20.4 $\mu g/cm^2$.

CO-stripping voltammograms were recorded by oxidizing pre-adsorbed CO (CO_{ad}) in 0.1 M $HClO_4$ at a potential scan rate of 50 mV/s. CO was purged into 0.1 M $HClO_4$ for 40 min to allow the equilibrium adsorption of CO on the deposited catalyst surfaces.

Results and discussion

Fig. 1 shows the representative TEM micrographs of Pt_3Ni nanoparticles supported on ((A) to (C)) rGO and ((D) to (F)) GCG, respectively. For the Pt_3Ni/rGO sample, in panel (A), one can see that a number of Pt_3Ni alloy nanoparticles, the dark-contrast objects, were dispersed rather evenly on a low-contrast sheet-like background of rGO. Higher-magnification images in panels (B) and (C) showed that the nanoparticles exhibited clearly-defined lattice fringes with an interlayer spacing of 1.96 Å and 2.24 Å (insets to panels (C) and (F)) that are consistent with the (200) and (111) crystallographic planes of face-centered cubic (fcc) Pt_3Ni alloy, respectively [17,31]. This suggests that DMF served as an effective reducing agent in the solvothermal synthesis of the Pt_3Ni/rGO nanocomposites, as observed previously [39,40]. Similar structural characteristics can be seen with Pt_3Ni–C/rGO, as manifested in panels (D) to (F). Note that the respective average diameter of the Pt_3Ni nanoparticles is rather consistent at 12.7 ± 2.5 nm and 12.6 ± 2.4 nm, based on statistical analysis of more than 100 nanoparticles in each sample, as manifested in the core size histograms (insets to panels (A) and (D)); and a large portion of the nanoparticles displayed a polyhedron-like shape, as highlighted by the red-dashed boxes in panels (B) and (E). Nevertheless, there is one apparent difference between Pt_3Ni–C/rGO and Pt_3Ni/rGO. In contrast to the rather uniform gray background in panel (A) of Pt_3Ni/rGO, the background of Pt_3Ni–C/rGO in panel (D) is rather uneven, with dark-gray globular objects (diameters range from 100 nm down to a few tens of nm) embedded in a light-gray background of reduced graphene oxide sheets. These were most likely carbon nanospheres that are embedded in the graphene nanosheet matrix (more TEM images in Fig. S1 in the Supporting Information).

The relative contents of Pt and Ni in Pt_3Ni/rGO and Pt_3Ni–C/rGO nanoparticles were then quantified by energy-dispersive X-ray spectroscopic (EDX) measurements. From the EDX spectra in the insets to panels (B) and (E), the molar ratio of Pt to Ni was estimated to be 2.9:1 and 3.0:1, respectively, consistent with the initial feed ratio of 3:1.

The crystalline structures of the Pt_3Ni/rGO and Pt_3Ni–C/rGO nanocomposites were then characterized by XRD measurements. From Fig. 2, one can see that both Pt_3Ni–C/rGO (curve a) and Pt_3Ni/rGO (curve b) exhibited four major peaks at $2\theta = 39.9°$, 46.3°, 68.1°, 81.6° and 85.7°, which are somewhat greater than those anticipated for the (111), (200), (220), (311) and (222) crystalline planes of *fcc* Pt (blue bars, PDF No. 65-2865), suggesting lattice shrinkage because of alloying with nickel in the nanoparticles [41]. From the width of the (111) diffraction peak, the size of the Pt_3Ni nanoparticles was estimated by the Scherrer equation to be 10.5 ± 0.2 nm for Pt_3Ni–C/rGO and 11.1 ± 0.3 nm for Pt_3Ni/rGO, respectively, in excellent agreement with the TEM results shown in Fig. 1. Furthermore, the absence of nickel diffraction features (brown bars, PDF No. 65-2865) indicates that no pure metallic nickel nanoparticles were formed in the samples.

One may also see that both Pt_3Ni/rGO and Pt_3Ni–C/rGO nanocomposites exhibited a broad peak centered at around 24.7°. This may be ascribed to diffraction from the graphite (002) crystalline planes. It should be noted that a similar feature can be observed with rGO (curve c), in contrast to GO that displayed only a diffraction peak at a much lower 2θ angle of 12.5° (curve d), implying that the graphene oxide sheets were mostly converted to highly conductive graphene after the solvothermal treatment.

The elemental compositions and charge states of the Pt_3Ni/rGO and Pt_3Ni–C/rGO nanocomposites were then examined by XPS measurements. As illustrated in the panels (A) and (D) of Fig. 3, the Pt4f electrons in both nanocomposites exhibited two pairs of peaks, one at 71.59 and 74.95 eV that may be attributed to the $4f_{7/2}$ and $4f_{5/2}$ electrons of metallic Pt, and the other at 71.98 and 75.38 eV that are consistent with PtO and PtOH species, respectively. For the Ni2p electrons in panels (B) and (E), deconvolution yields a major peak at 853.23 eV and a satellite at 860.83 eV that are consistent with metallic Ni, as well as two additional peaks centered at 854.63 eV and 856.63 eV that may be attributed to NiO and $Ni(OH)_2$, respectively. Note that the presence of metal oxides has been suggested to not only facilitate the formation of surface hydroxyl species and transport of protons and electrons that are essential in methanol oxidation but also prevent the catalysts from corrosion [42]. For the C1s electrons in panels (C) and (F), three main peaks were identified at 284.73 eV, 285.58 eV and

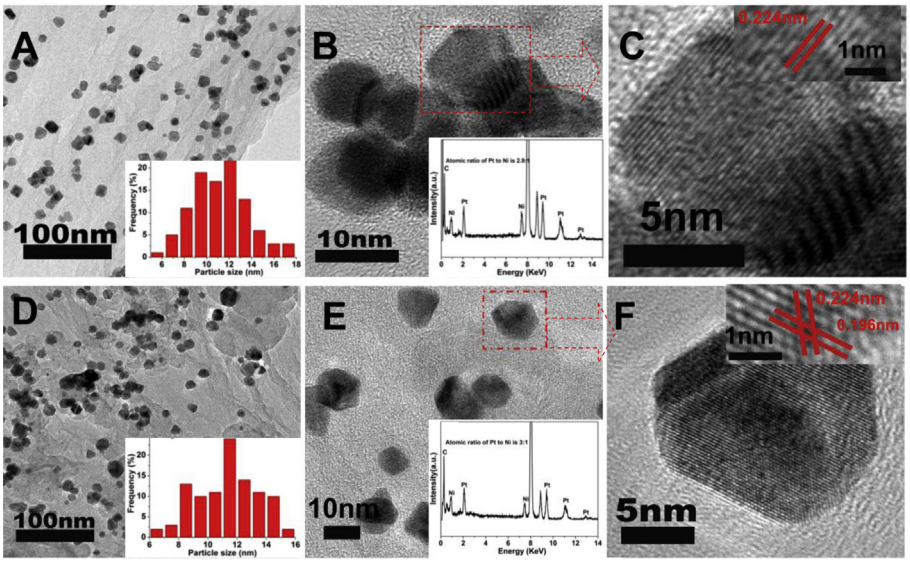

Fig. 1 – Representative TEM images of Pt_3Ni/rGO (A, B, and C) and Pt_3Ni–C/rGO (D, E, and F) nanocomposites. Panels (C) and (F) are the zoom-in of the particles highlighted by the red boxes in panels (B) and (E), respectively. Insets to panels (A) and (D) are the corresponding core size histograms, insets to panels (B) and (E) are the respective EDX spectrum, and insets to panels (C) and (F) are the corresponding high-resolution images with red lines representing crystalline lattice fringes. (For interpretation of the references to color in this figure legend, the reader is referred to the web version of this article.)

288.07 eV that may be assigned to carbons in C–C/C=C, C–O, and C=O, respectively, at an atomic ratio of 2.01:1.23:1. One may also notice that the binding energies of the Pt4f and Ni2p electrons in Pt_3Ni are somewhat higher than those of standard Pt(0) (71.3 eV and 74.4 eV) and Ni(0) (852.70 eV), suggesting electron transfer likely occurred from Pt_3Ni nanoparticles to graphene oxide [43–45]. This may lead to reduced binding energy of Pt–CO and hence weakened the adsorption of CO on Pt_3Ni nanoparticle surfaces [46–50], as manifested in electrochemical measurements below.

Raman measurements were then carried out to further examine the carbon supporting substrates, as depicted in Fig. 4. It can be seen that GO, rGO, Pt_3Ni/rGO, and Pt_3Ni–C/rGO all exhibited a pair of peaks at 1585 cm^{-1} and 1348 cm^{-1}. The

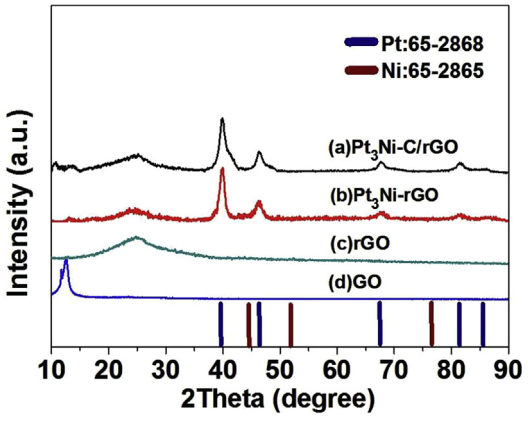

Fig. 2 – XRD patterns of the as-prepared GO, rGO, Pt_3Ni/rGO, Pt_3Ni–C/rGO composites.

former may be assigned to the G band that is related to the vibration of sp^2-bonded carbon atoms, whereas the latter is known as the D band, which usually originates from vibrations of carbon atoms with dangling bonds defects and staging disorder in the plane of graphene sheets. Furthermore, the ratio between the D and G band intensity (I_D/I_G) for the Pt_3Ni–C/rGO catalysts was estimated to be 1.07, somewhat greater than those for Pt_3Ni/rGO (1.01), rGO (0.98) and GO (0.96), suggesting enhanced disordering with the insertion of carbon nanospheres into the rGO sheets.

Electrochemical measurements were then carried out to examine the electrocatalytic activity of the nanocomposites in methanol oxidation. Fig. 5 shows the cyclic voltammograms of a glassy carbon electrode modified with a same amount of (black curve) rGO and (red curve) GCG in 0.1 M $HClO_4$ at a potential scan rate of 50 mV/s. It can be seen that both electrodes exhibited a pair of voltammetric peaks at ca. +0.70 V. This most likely arose from redox reactions of oxygen-containing functional groups on graphene surfaces. The markedly higher peak currents of the GCG-modified electrode suggested that the effective electrochemical surface area of GCG was greater than that of rGO. A consistent behavior can be seen with the double-layer charging currents, with a notably broader charging envelope for GCG than for rGO. These results suggest that with the insertion of carbon spheres in between the graphene sheets, the restacking and refolding of graphene sheets was minimized during the solvothermal process. This facilitated the access of the electrolyte species to the internal structures of the carbon support, leading to a dramatic increase of the electrochemically accessible surface area (ECSA) due to the unique 3D sandwich-like structure [51,52].

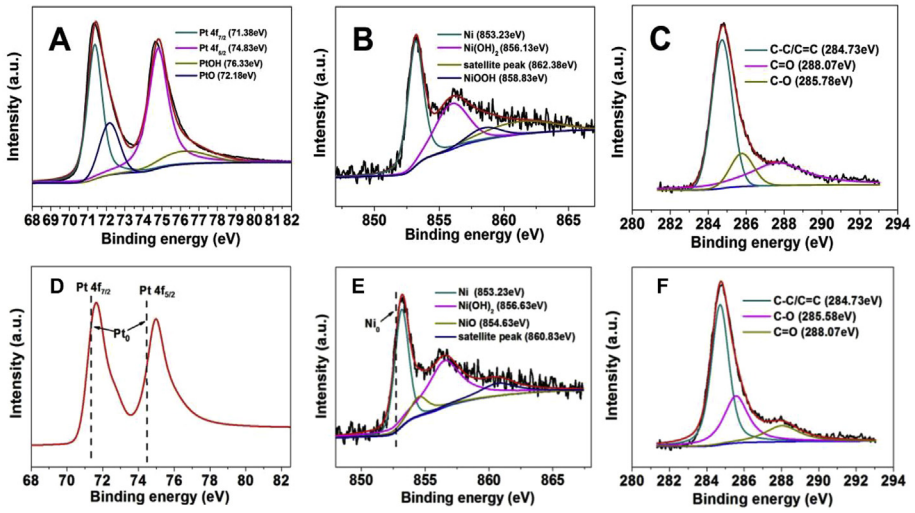

Fig. 3 – XPS spectra of (A, D) Pt 4f, (B, E) Ni 2p, (C, F) C1s electrons in (A to C) Pt_3Ni/rGO and (D to F) Pt_3Ni–C/rGO composites. Black curves are the plots of experimental data and the color curves are deconvolution fits. (For interpretation of the references to color in this figure legend, the reader is referred to the web version of this article.)

The electrocatalytic activity in methanol oxidation was then evaluated. Fig. 6(A) shows the cyclic voltammograms of the Pt/C, Pt_3Ni/rGO and Pt_3Ni–C/rGO catalysts loaded onto a glassy carbon electrode at a scan rate of 50 mV/s in 0.1 M $HClO_4$ + 1.0 M CH_3OH. It can be seen that for all nanoparticle catalysts, in the anodic scan oxidation currents started to emerge at potentials around +0.60 V, and reached the peak values at a more positive potential of around +0.93 V; in the reverse scan, a similar anodic voltammetric peak can be seen but at a less positive potential around +0.75 V, suggesting effective catalytic oxidation of methanol by these nanoparticle catalysts. Yet, a careful analysis shows that the onset potential of methanol oxidation actually increased in the order of Pt_3Ni–C/rGO (+0.65 V) < Pt/C (+0.68 V) < Pt_3Ni/rGO (+0.70 V); and the current density at +0.93 V is 360.4 mA/mg for Pt_3Ni–C/rGO, nearly 1.7 and 1.3 times higher than those on Pt_3Ni/rGO (210.7 mA/mg) and commercial Pt/C (267.8 mA/mg), respectively. In addition, it is worthy to note that in the anodic scan the Pt_3Ni–C/rGO catalyst also shows a somewhat lower peak potential and higher peak current density than those reported by Li et al. [41] with Pt_3Ni/rGO (+0.96 V, 145.8 mA/mg) and Chen et al. [8] with PtPd/rGO (+0.97 V, 198.0 mA/mg). With respect to the specific activity, in the present study, the Pt_3Ni–C/rGO catalyst (0.66 mA/cm^2) is 1.3- and 1.2-times more active than Pt_3N/rGO (0.51 mA/cm^2) and commercial Pt/C (0.54 mA/cm^2), respectively (Fig. 6(B)). These observations explicitly demonstrate that the Pt_3Ni–C/rGO displays the highest catalytic activity in the electrooxidation of methanol among the series of catalysts in the present study. Nevertheless, it should be noted that the performance of the above-mentioned Pt_3Ni–C/rGO is not yet as good as that of "state of the art" PtRu catalysts. However, simple addition of carbon spheres into the rGO substrates clearly enhanced the electrochemical surface area and hence the accessibility of

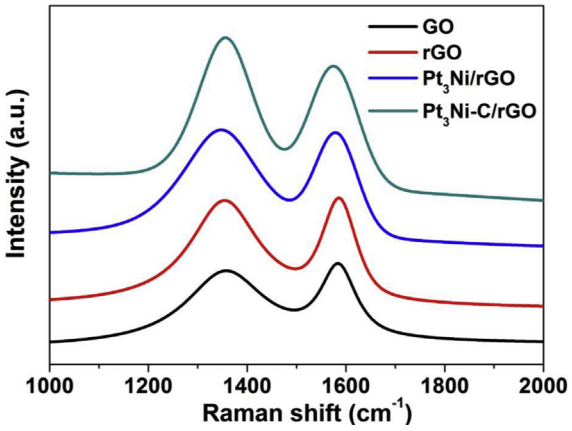

Fig. 4 – Raman spectra of GO, rGO, Pt_3Ni/rGO, and Pt_3Ni–C/rGO.

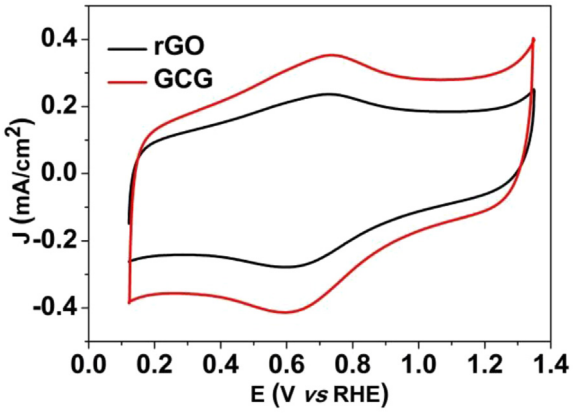

Fig. 5 – Cyclic voltammograms of a glassy carbon electrode modified with a same amount (15 μg) of rGO and GCG in 0.1 M $HClO_4$. Electrode surface area 0.196 cm^2; potential scan rate 50 mV/s.

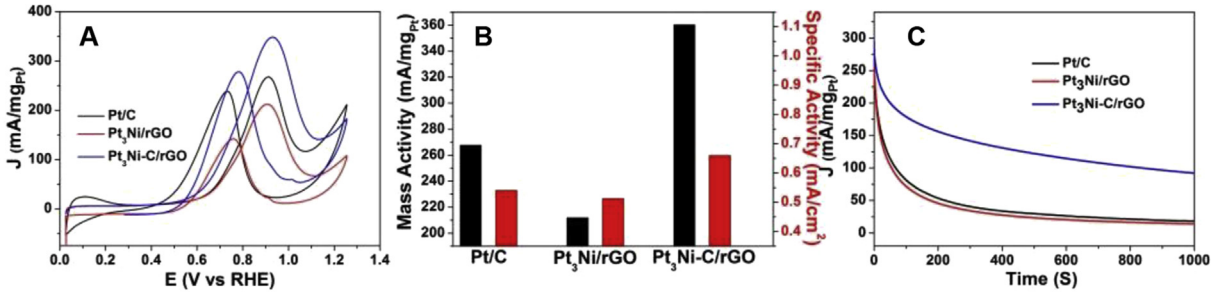

Fig. 6 – (A) cyclic voltammograms of a glassy carbon electrode (0.196 cm^2) modified with Pt$_3$Ni–C/rGO, Pt$_3$Ni/rGO, and Pt/C in 0.1 M HClO$_4$ + 1 M CH$_3$OH. Potential scan rate 50 mV/s. (B) Comparsion of the specific activity at +0.93 V. (C) Chronoamperometric curves recorded at +0.95 V in 0.1 M HClO$_4$ + 1 M CH$_3$OH. Pt loading was 20.4 μg/cm^2 for all samples.

nanoparticle catalyst surface, a strategy that might be exploited as a generic and effective mechanism for the further enhancement of nanoparticle electrocatalytic activity in methanol oxidation.

Note that in the above analysis, the effective electrochemical surface area (ECSA) was quantified by CO stripping measurement within the potential range of +0.6 to +1.0 V, as depicted in Fig. 7, which was observed to increase in the order of Pt$_3$Ni/rGO (42.8 m^2/g) < commercial Pt/C (50.1 m^2/g) < Pt$_3$Ni–C/rGO (52.7 m^2/g). One may note that whereas the particle size of Pt$_3$Ni in Pt$_3$Ni/rGO and Pt$_3$Ni–C/rGO is almost identical, the ECSA of Pt$_3$Ni–C/rGO is markedly larger than that of Pt$_3$Ni/rGO. This might be accounted for, again, by the insertion of carbon nanospheres into the graphene nanosheet matrix forming the GCG sandwich-like structure that likely prevented the restacking/refolding of the graphene sheets and generated an increasing number of accessible active sites as well as transport channels for mass and charges. These unique features are beneficial to the catalytic reactions. Moreover, whereas the core size of the Pt$_3$Ni nanoparticles prepared above is markedly larger than that of commercial Pt/C (*ca.* 3.3 nm) [46], the ECSA of Pt$_3$Ni–C/rGO is actually higher, as a result of the polyhedral shape of the Pt$_3$Ni nanoparticles as well as enhanced surface accessibility by the insertion of carbon spheres into the graphene support. Similar behaviors have also been observed previously [20,53].

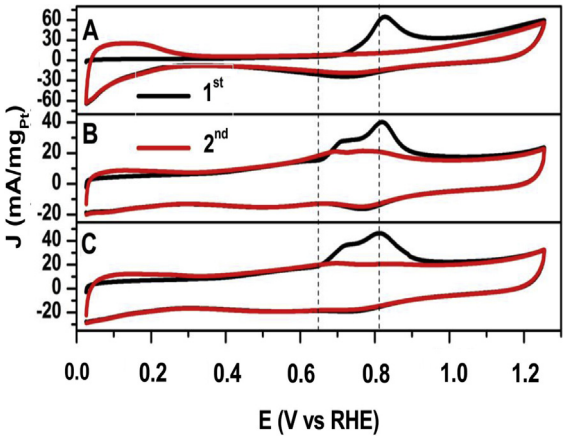

Fig. 7 – The first (black curves) and second (red curves) cyclic voltammograms of a glassy carbon electrode (0.196 cm^2) modified with (A) commercial Pt/C, (B) Pt$_3$Ni/rGO, and (C) Pt$_3$Ni–C/rGO catalysts that was initially covered by an adsorbed layer of CO in 0.1 M HClO$_4$. Potential scan rate was 50 mV/s. Pt loading was all 20.4 μg/cm^2. (For interpretation of the references to color in this figure legend, the reader is referred to the web version of this article.)

Tolerance to poisonous species is also of great importance for catalysts in practical applications. It is well known that when methanol is oxidized on Pt-based catalysts, poisonous intermediates, such as CHO$_{ads}$ and CO$_{ads}$, may be formed and strongly absorbed on the platinum surfaces, leading to self–poisoning of the catalysts [45]. The ratio of the oxidation peak current density in the anodic and cathodic scans (J_f/J_b) is generally used to quantitatively evaluate the tolerance strength of the catalysts to CO poisoning. A higher J_f/J_b value suggests stronger CO tolerance of the catalyst. Based on the data in Fig. 6(A), the J_f/J_b ratio of Pt$_3$Ni–C/rGO and Pt$_3$Ni/rGO is estimated to be 1.25 and 1.43, respectively, both markedly higher than that of Pt/C (1.11), again suggesting enhanced CO tolerance of the catalysts.

Stability is another critical factor in the assessments of nanoparticle catalysts. Fig. 6(C) shows the chronoamperometric (CA) profiles recorded at +0.85 V in 0.1 M HClO$_4$ + 1.0 M CH$_3$OH with the same catalysts-modified electrodes. Although all catalysts show a rapid decrease of the voltammetric currents (at roughly the same decay rate), the Pt$_3$Ni–C/rGO catalysts maintained a much higher current than the other two catalysts, demonstrating remarkably enhanced electrocatalytic activity and stability. For instance, after 600 s of operation, the current density of Pt$_3$Ni–C/rGO was 114.7 mA/mg, whereas only 20.4 mA/mg and 26.4 mA/mg were observed for Pt$_3$Ni/rGO and commercial Pt/C, respectively.

CO stripping is another commonly used method to assess the resistance of Pt-based catalysts to CO in methanol oxidation [35]. Fig. 7 shows the cyclic voltammograms of a glassy-carbon electrode modified with (A) Pt/C, (B) Pt$_3$Ni/rGO, and (C) Pt$_3$Ni–C/rGO nanoparticles that was covered with an adsorbed layer of CO in a HClO$_4$ solution. The hydrogen desorption peak almost completely disappeared in the first positive-going scan (black curves) because the active sites had been occupied by pre-adsorbed CO. However, a broad current peak was generated in the potential range of +0.6 V

to +1.0 V, which was attributed to the oxidative removal of adsorbed CO, and consequently the hydrogen adsorption/desorption peaks were recovered in the second scans (red curves). The potential of CO oxidation is another important factor in the evaluation of CO tolerance. It can be seen from Fig. 7 that CO oxidation on (C) Pt_3Ni–C/rGO peaked at ca. +0.81 V, markedly more negative than that of (A) Pt/C (+0.83 V) and (B) Pt_3Ni/rGO (+0.82 V). Additionally, the onset potential of CO oxidation on Pt_3Ni–C/rGO is +0.65 V, which is also lower than those of commercial Pt/C (+0.71 V) and Pt_3Ni/rGO (+0.68 V). These results further highlight the excellent CO tolerance ability of Pt_3Ni–C/rGO catalysts, which is likely due to the relatively weak bonding of Pt–CO resulting from electron transfer from Pt_3Ni to reduced graphene oxide as manifested in XPS measurements (Fig. 3). The observation is consistent with the chronoamperometric profiles shown in Fig. 6(C), where the decay rate of Pt_3Ni–C/rGO was the lowest among the series (Table S1).

One may notice that in contrast to Pt/C in panel (A), both Pt_3Ni catalysts in panels (B) and (C) actually exhibited two voltammetric peaks. This may be attributed to the complexity of adsorption sites of CO on the surfaces of Pt_3Ni alloy nanoparticles, where the peak at the lower potential is likely due to the oxidation of CO adsorbed on Pt (110) planes or edge sites of the Pt (111) planes, while the peak at the higher potential to the oxidation of CO adsorbed on Pt (111) planes [54].

Conclusions

In summary, a facile strategy was described for the synthesis of Pt_3Ni alloy nanoparticles supported on graphene/carbon nanospheres sandwich-like substrates (Pt_3Ni–C/rGO). The resulting nanocomposites exhibited markedly enhanced electrocatalytic activity and much improved durability in methanol oxidation reaction as compared to commercial Pt/C catalysts and Pt_3Ni nanoparticles supported on graphene nanosheets alone (Pt_3Ni/rGO). Experimental measurements showed that the superior catalytic activity might be attributed to the unique sandwich-like structure of the supporting substrate that increased the effective electrochemical surface area of Pt_3Ni nanoparticles and hence the transport of electrolyte ions and reactant/product molecules. Mechanistically, the markedly enhanced CO tolerance of Pt_3Ni–C/rGO was likely due to a decreased electron density of the Pt_3Ni nanoparticles with partial electron transfer to graphene sheets that weakened the interactions with CO. Such a strategy might be exploited as an effective mechanism in the design and engineering of nanoparticle catalysts for enhanced performance.

Acknowledgments

This work was supported by the National Recruitment Program of Global Experts. L.G.L acknowledges the financial support from the Fundamental Research Funds for the Central Universities (SCUT Grant No. 2013ZM0019). S. W. C. acknowledges support from the National Science Foundation (CHE-1265635 and DMR-1409396).

Appendix A. Supplementary data

Supplementary data related to this article can be found at http://dx.doi.org/10.1016/j.ijhydene.2015.02.095.

REFERENCES

[1] Chen YX, Miki A, Ye S, Sakai H, Osawa M. Formate, an active intermediate for direct oxidation of methanol on Pt electrode. J Am Chem Soc 2003;125:3680–1.
[2] Liang HP, Zhang HM, Hu JS, Guo YG, Wan LJ, Bai CL. Pt hollow nanospheres: facile synthesis and enhanced electrocatalysts. Angew Chem Int Ed 2004;43:1540–3.
[3] Wang HL, Wang YH, Zhu ZW, Sapi A, An KJ, Kennedy G, et al. Influence of size-induced oxidation state of platinum nanoparticles on selectivity and activity in catalytic methanol oxidation in the gas phase. Nano Lett 2013;13:3966.
[4] Alia SM, Zhang G, Kisailus D, Li DS, Gu S, Jensen K, et al. Porous platinum nanotubes for oxygen reduction and methanol oxidation reactions. Adv Func Mater 2010;20:3742–6.
[5] Chen DH, Zhao YC, Fan YF, Wang WL, Li XX, Peng XL, et al. Preparation and characterization of core-shell-like PbPt nanoparticles electro-catalyst supported on graphene for methanol oxidation. Int J Hydrogen Energy 2014;39:16053–60.
[6] Ye WC, Kou HH, Liu QZ, Yan JF, Zhou F, Wang CM. Electrochemical deposition of Au–Pt alloy particles with cauliflower-like microstructures for electrocatalytic methanol oxidation. Int J Hydrogen Energy 2012;37:4088–97.
[7] Wang RF, Wang H, Wei BX, Wang W, Lei ZQ. Carbon supported Pt-shell modified PdCo-core with electrocatalyst for methanol oxidation. Int J Hydrogen Energy 2010;35:10081–6.
[8] Sieben JM, Duarte MME, Mayer CE. Methanol oxidation on carbon supported Pt–Ru catalysts prepared by electrodeposition – evaluation of nafion (R) 117 film effect. Int J Hydrogen Energy 2010;35:2018–24.
[9] Kim DB, Chun HJ, Lee YK, Kwon HH, Lee HI. Preparation of Pt/NiO–C electrocatalyst and heat-treatment effect on its electrocatalytic performance for methanol oxidation. Int J Hydrogen Energy 2010;35:313–20.
[10] Qiu HJ, Huang XR. Nanoporous PtFe surface alloy architecture for enhanced methanol electro-oxidation (Retraction of vol. 22, pg 7602, 2012). J Mater Chem 2012;22:25504.
[11] Nassr AAA, Sinev I, Pohl MM, Grunert W, Bron M. Rapid microwave-assisted polyol reduction for the preparation of highly active PtNi/CNT electrocatalysts for methanol oxidation. Acs Catal 2014;4:2449–62.
[12] Sun SJ, Gao QM. Enhanced methanol electro-oxidation activity of PtNi alloy nanoparticles on the large surface area porous carbon. Rare Met 2011;30:42–7.
[13] Liu F, Lee JY, Zhou WJ. Template preparation of multisegment PtNi nanorods as methanol electro-oxidation catalysts with adjustable bimetallic pair sites. J Phys Chem B 2004;108:17959–63.
[14] Deivaraj TC, Chen WX, Lee JY. Preparation of PtNi nanoparticles for the electrocatalytic oxidation of methanol. J Mater Chem 2003;13:2555–60.

[15] Cui XZ, Shi JL, Zhang LX, Ruan ML, Gao JH. PtCo supported on ordered mesoporous carbon as an electrode catalyst for methanol oxidation. Carbon 2009;47:186–94.
[16] Huang YY, Cai JD, Guo YL. Facile synthesis of a Bi-modified PtRu catalyst for methanol and ethanol electro-oxidation in alkaline medium. Int J Hydrogen Energy 2013;38:3250–6.
[17] Wu JB, Qi L, You HJ, Gross A, Li J, Yang H. Icosahedral platinum alloy nanocrystals with enhanced electrocatalytic activities. J Am Chem Soc 2012;134:11880–3.
[18] Hwang SJ, Kim SK, Lee JG, Lee SC, Jang JH, Kim P, et al. Role of electronic perturbation in stability and activity of Pt-based alloy nanocatalysts for oxygen reduction. J Am Chem Soc 2012;134:19508–11.
[19] Stamenkovic VR, Fowler B, Mun BS, Wang G, Ross PN, Lucas CA, et al. Improved oxygen reduction activity on $Pt_3Ni(111)$ via increased surface site availability. Science 2007;315:493–7.
[20] Carpenter MK, Moylan TE, Kukreja RS, Atwan MH, Tessema MM. Solvothermal synthesis of platinum alloy nanoparticles for oxygen reduction electrocatalysis. J Am Chem Soc 2012;134:8535–42.
[21] Gao H, Xiao F, Ching CB, Duan H. One-step electrochemical synthesis of PtNi nanoparticle-graphene nanocomposites for nonenzymatic amperometric glucose detection. ACS Appl Mater &Inter 2011;3:3049–57.
[22] Pillay D, Johannes MD. Effect of S on Pt(111) and $Pt_3Ni(111)$ surfaces: a first principles study. J Phys Chem C 2008;112:1544–51.
[23] Zhang J, Yang HZ, Fang JY, Zou SZ. Synthesis and oxygen reduction activity of shape-controlled Pt_3Ni nanopolyhedra. Nano Lett 2010;10:638–44.
[24] Huang X, Zhu E, Chen Y, Li Y, Chiu C-Y, Xu Y, et al. A facile strategy to Pt_3Ni nanocrystals with highly porous features as an enhanced oxygen reduction reaction catalyst. Adv Mater 2013;25:2974–9.
[25] Park KW, Choi JH, Kwon BK, Lee SA, Sung YE, Ha HY, et al. Chemical and electronic effects of Ni in Pt/Ni and Pt/Ru/Ni alloy nanoparticles in methanol electrooxidation. J Phys Chem B 2002;106:1869–77.
[26] Antolini E, Salgado JRC, Gonzalez ER. The methanol oxidation reaction on platinum alloys with the first row transition metals – the case of Pt–Co and –Ni alloy electrocatalysts for DMFCs: a short review. Appl Catal B-Environ 2006;63:137–49.
[27] Guo SJ, Dong SJ, Wang EK. Three-dimensional Pt-on-Pd bimetallic nanodendrites supported on graphene nanosheet: facile synthesis and used as an advanced nanoelectrocatalyst for methanol oxidation. Acs Nano 2010;4:547–55.
[28] Jeong GH, Kim SH, Kim M, Choi D, Lee JH, Kim JH, et al. Direct synthesis of noble metal/graphene nanocomposites from graphite in water: photo-synthesis. Chem Commun 2011;47:12236–8.
[29] Hiramatsu H, Osterloh FE. A simple large-scale synthesis of nearly monodisperse gold and silver nanoparticles with adjustable sizes and with exchangeable surfactants. Chem Mater 2004;16:2509–11.
[30] Fang B, Chaudhari NK, Kim MS, Kim JH, Yu JS. Homogeneous deposition of platinum nanoparticles on carbon black for proton exchange membrane fuel cell. J Am Chem Soc 2009;131:15330–8.
[31] Li WZ, Liang CH, Zhou WJ, Qiu JS, Zhou ZH, Sun GQ, et al. Preparation and characterization of multiwalled carbon nanotube-supported platinum for cathode catalysts of direct methanol fuel cells. J Phys Chem B 2003;107:6292–9.
[32] Li Y, Li Y, Zhu E, McLouth T, Chiu C-Y, Huang X, et al. Stabilization of high-performance oxygen reduction reaction Pt electrocatalyst supported on reduced graphene oxide/carbon black composite. J Am Chem Soc 2012;134:12326–9.
[33] Tan YM, Xu CF, Chen GX, Zheng NF, Xie QJ. A graphene-platinum nanoparticles-ionic liquid composite catalyst for methanol-tolerant oxygen reduction reaction. Energy Environ Sci 2012;5:6923–7.
[34] Xu PF, Dong L, Neek-Amal M, Ackerman ML, Yu JH, Barber SD, et al. Self-organized platinum nanoparticles on freestanding graphene. ACS Nano 2014;8:2697–703.
[35] Lu YZ, Jiang YY, Wu HB, Chen W. Nano-PtPd cubes on graphene exhibit enhanced activity and durability in methanol electrooxidation after CO stripping-cleaning. J Phys Chem C 2013;117:2926–38.
[36] Huang XQ, Tang SH, Mu XL, Dai Y, Chen GX, Zhou ZY, et al. Freestanding palladium nanosheets with plasmonic and catalytic properties. Nat Nanotech 2011;6:28–32.
[37] Kang YJ, Ye XC, Murray CB. Size- and shape-selective synthesis of metal nanocrystals and nanowires using CO as a reducing agent. Angew Chem Int Ed 2010;49:6156–9.
[38] Cote LJ, Kim F, Huang JX. Langmuir-Blodgett assembly of graphite oxide single layers. J Am Chem Soc 2009;131:1043–9.
[39] Lu Y, Jiang Y, Chen W. Graphene nanosheet-tailored PtPd concave nanocubes with enhanced electrocatalytic activity and durability for methanol oxidation. Nanoscale 2014;6:3309–15.
[40] Chen X, Cai Z, Chen X, Oyama M. Synthesis of bimetallic PtPd nanocubes on graphene with N,N-dimethylformamide and their direct use for methanol electrocatalytic oxidation. Carbon 2014;66:387–94.
[41] Li LH, Wu Y, Lu J, Nan CY, Li YD. Synthesis of Pt–Ni/graphene via in situ reduction and its enhanced catalyst activity for methanol oxidation. Chem Commun 2013;49:7486–8.
[42] Kowal A, Port SN, Nichols RJ. Nickel hydroxide electrocatalysts for alcohol oxidation reactions: an evaluation by infrared spectroscopy and electrochemical methods. Catal Today 1997;38:483–92.
[43] Chen XM, Cai ZX, Chen X, Oyama M. Green synthesis of graphene-PtPd alloy nanoparticles with high electrocatalytic performance for ethanol oxidation. J Mater Chem A 2014;2:315–20.
[44] Jiang QA, Jiang LH, Hou HY, Qi J, Wang SL, Sun GQ. Promoting effect of Ni in PtNi bimetallic electrocatalysts for the methanol oxidation reaction in alkaline media: experimental and density functional theory studies. J Phys Chem C 2010;114:19714–22.
[45] Zhang K, Yue QL, Chen GF, Zhai YL, Wang L, Wang HS, et al. Effects of acid treatment of Pt-Ni alloy nanoparticles@graphene on the kinetics of the oxygen reduction reaction in acidic and alkaline solutions. J Phys Chem C 2011;115:379–89.
[46] Zhou ZY, Kang XW, Song Y, Chen SW. Ligand-mediated electrocatalytic activity of Pt nanoparticles for oxygen reduction reactions. J Phys Chem C 2012;116:10592–8.
[47] Sen F, Gokagac G. Different sized platinum nanoparticles supported on carbon: an XPS study on these methanol oxidation catalysts. J Phys Chem C 2007;111:5715–20.
[48] Wakisaka M, Mitsui S, Hirose Y, Kawashima K, Uchida H, Watanabe M. Electronic structures of Pt–Co and Pt–Ru alloys for Co-tolerant anode catalysts in polymer electrolyte fuel cells studied by EC-XPS. J Phys Chem B 2006;110:23489–96.
[49] Uchida H, Izumi K, Watanabe M. Temperature dependence of CO-tolerant hydrogen oxidation reaction activity at Pt,

Pt–Co, and Pt–Ru electrodes. J Phys Chem B 2006;110:21924–30.
[50] Chen DH, Zhao YC, Fan YF, Peng XL, Wang X, Tian JN. Synthesis of Ni@PbPt supported on graphene by galvanic displacement reaction for improving ethanol electro-oxidation. J Mater Chem A 2013;1:13227–32.
[51] Wu G, Chen YS, Xu BQ. Remarkable support effect of SWNTs in Pt catalyst for methanol electro oxidation. Electrochem Commun 2005;7:1237–43.
[52] Zhou YK, He BL, Zhou WJ, Huang J, Li XH, Wu B, et al. Electrochemical capacitance of well-coated single-walled carbon nanotube with polyaniline composites. Electrochim Acta 2004;49:257–62.
[53] Cui CH, Gan L, Li HH, Yu SH, Heggen M, Strasser P. Octahedral PtNi nanoparticle catalysts: exceptional oxygen reduction activity by tuning the alloy particle surface composition. Nano Lett 2012;12:5885–9.
[54] Chen C-S, Pan F-M. Electrocatalytic activity of Pt nanoparticles deposited on porous TiO_2 supports toward methanol oxidation. Appl Catal B 2009;91:663–70.